

3D SUBSURFACE IMAGING OF PRECIPITATES INSIDE BLOCK-CAST SILICON

S. Köstner¹, H. Cypionka², H. van der Voort³, J. Bauer¹, J.-M. Wagner¹, O. Breitenstein¹

¹Max-Planck-Institut für Mikrostrukturphysik, Weinberg 2, 06120 Halle, Germany

²Universität Oldenburg, Ammerländer Heerstraße 114-118, D-26129 Oldenburg

³Scientific Volume Imaging bv, Laapersveld 63, 1213 VB Hilversum, The Netherlands

ABSTRACT: SiC filaments are known to cause severe ohmic shunts in mc-Si solar cells. However, not all of them contribute to ohmic shunting. In order to obtain information on how the SiC filaments are embedded inside the bulk material, we demonstrate a novel method which reveals the 3d geometry of the embedded structures at high resolution (below 1 micron). This method is based on an improved algorithm for extended depth-of-focus imaging, evaluating a stack of about 50 IR microscopy images by considering their local contrast. For comparison, a commercial deconvolution algorithm with a depth-dependent point-spread function is used. The resulting 3d images permit the electrical characterization of embedded SiC filaments, knowing exactly their geometry. Further, new insights on the growing mechanisms of SiC filaments can be expected.

Keywords: multi-crystalline silicon, precipitates, IR microscopy, subsurface imaging

1 INTRODUCTION

Solar cells made from multi-crystalline Silicon (mc-Si) regularly suffer from “shunts”, which are leading to leakage currents, thereby reducing their fill factor (FF) and open circuit voltage (V_{oc}). Shunts can be detected best by Lock-In Thermography (LIT) due to Joule type heat dissipation [1]. Combined with microstructural investigations meanwhile many different shunting mechanisms have been identified [2]. Among the most prominent are material-induced shunts due to SiC precipitates and inclusions.

Precipitates, mostly appearing in the uppermost parts of block-cast Si, have been intensively investigated by infrared microscopy (IRM) at low resolution (x50) or chemically dissolving them from the surrounding Si material. [3,4] SiC filaments, heavily n-doped by nitrogen, have been identified as the main cause for severe ohmic shunting. [5,6] However, it was observed that not all filaments contribute to ohmic shunting. Figure 1 shows a LIT image overlaid by an IRM image. Not all precipitates show a strong thermal signal under LIT. S2 and S3 appear to be heavy shunting whereas the thermal signal in K4 appears to be less enhanced. Other precipitates do not show a signal at all, mainly due to their horizontal orientation or their small size or because they are non-conducting.

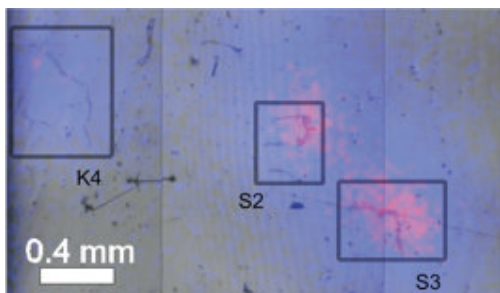


Figure 1: Infrared microscopy overlaid with LIT image to distinguish shunting from non-shunting precipitates.

So far the electrical properties of the SiC filaments were determined without having any information on how they are embedded inside the bulk material. In this paper we demonstrate a method which reveals for the very first

time the three dimensional geometry of these structures at high resolution (below 1 micron) while they are still embedded inside the cells.

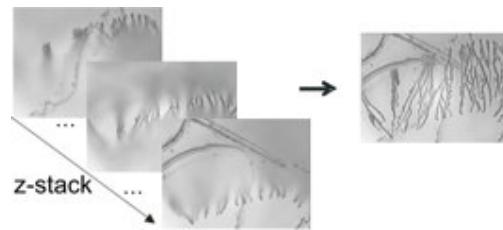


Figure 2: Images taken at different focus levels with high numerical aperture can be fused together numerically to an extended depth of focus image. Images taken with a Si CCD of 768*573 pixel. Picolay fusion algorithm was used [8].

IR microscopy with high numerical apertures above 0.8 can be used for taking a stack of images at different heights inside the substrate. The depth of focus d of each slide is proportional to:

$$d = \lambda n / NA^2$$

By means of numeric algorithms the various images (about 50) can be fused together to an extended depth of focus image, as demonstrated in Figure 2. By restoring the additionally gained z-information, 3d images can be reconstructed. Stereoscopic projections can be obtained, to be viewed with 3d goggles, as well as volume rendered images, to be viewed as tomography-like animations.

This method will permit electrical characterization of embedded SiC filaments while knowing exactly their 3d geometry inside the solar cell. Further, new insights on the growing mechanisms of SiC filaments can be expected.

2 NUMERIC ALGORITHMS

Many different numeric algorithms, in the object space as well as Fourier space, have been introduced since the easy availability of the necessary computational power in the 80's, mainly with the goal to extend the depth of focus in high resolution microscopy. A

comparison and overview of some of them is given in [7]. In this paper we present an algorithm which is based on the local contrast of an image, which to the best of the author's knowledge, by now has grown to become one of the fastest of its kind [8]. Dealing with a more complex parameter space, a commercial software was evaluated [9]. The fusion process in this package is based on the deconvolution of the point spread function of the microscope.

2.1 Local contrast based image fusion

Algorithms in object space are normally categorized into two different classes of methods: the point-based methods, where pixels with the same x,y-coordinates are compared with each other along the z-axis to be selected upon a maximum or minimum selection rule [10, 11] and neighborhood-based methods, where the neighborhood of each pixel is taken into account to identify in-focus areas [12,13]. Picolay [8] intuitively combines both approaches and implements an edge detection procedure, for identifying sharp areas, that can be summarized as follows.

Although not important for IRM in the first step the RGB values are combined to a weighted greyvalue with the ratios: red 30%, green 59% and blue 11%, to respect the spectral sensitivity of the human eye. In the next step for each pixel m the micro-contrast (MC) is evaluated, which is the summed variance to the next neighbors, forming horizontal, vertical and diagonal pairs, which can be written as

$$MC = \sum_i ((n_{i,l} - n_{i,r}) - m \times 2)$$

Where $n_{i,l}$ and $n_{i,r}$ denote the left and right next neighbors of m as well as up and down for the vertical pair of neighbors. In the next step the contrast map, C , is calculated. Based on the micro-contrast values of the neighboring pixels it is calculated as a weighted sum over the neighboring MC values:

$$C = \mu \times 32 + \sum \alpha_i \times 2 + \sum \beta_i \times 2$$

Integers are used as weighting factors to improve processing speed. For better understanding the procedure for calculating micro-contrast and contrast, the involved matrices are visualized again in Figure 3, respectively.

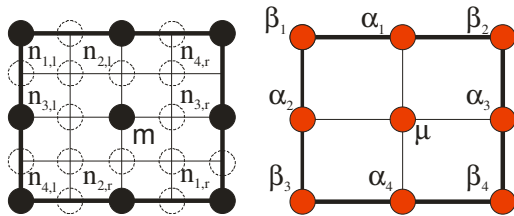


Figure 3: On the left hand side the micro-contrast matrix is shown. Black dots are indicating the next-neighboring pairs. The open circles are representing the neighbouring pixels. The red dots on the right image are indicating the micro-contrast values which form the basis for the contrast calculation. The horizontal pair of neighbors is grouped with the vertical pair and weighted with 3 whereas the diagonal pairs are weighted with 2.

Having calculated the contrast map in each layer a threshold can be applied. Pixels above this threshold are

compared along the z-axis. The pixel with the maximum contrast is allocated for the fused extended depth of focus image.

Picolay has proven to be a fast and efficient edge detection algorithm, however difficulties arise when it had to deal with larger in-focus areas, due to lack of contrast. Resizing the various matrices for micro-contrast and contrast reduces artefacts, however at the cost of resolution. A more elegant solution to overcome this problem, without losing resolution, is to downscale the image in a first iteration. The contrast map is expanded again after processing and compared with the result of the normal-sized image. In case the difference in contrast is higher than a threshold, the pixel value from the downscaled image is allocated.

For comparison a color based stacking algorithm is implemented which can be categorized as a point-like method. In this approach it is looked for the pixel closest to the target color at a given x,y coordinate. This algorithm works well with images of high contrast, as in the ideal case the filaments appear as black on a white background. Therefore it is probably the fastest approach possible and is especially suitable for high resolution images. An image of a 2048*2048 pixel CCD camera is shown in Figure 4.

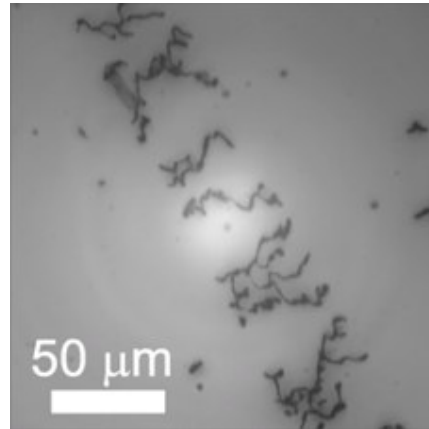


Figure 4: Extended depth of focus image of filaments taken with 2048*2048 pixel resolution. Color based image fusion was applied.

2.2 Deconvolution of the point spread function

The impressive increase of computation power of multi-core machines in recent years and the success of PC-farms allow for computationally more intensive algorithms. A model based approach is the deconvolution of the point spread function.

An optically linear system like an incoherent widefield microscope, can be entirely described by its point spread function (PSF). In the case of IRM brightfield images which are partially coherent, the imaging of high contrast objects can be considered sufficiently linear to be described by convolution with a PSF [14]. The Huygens Software of Scientific Volume imaging [9] enables to obtain a PSF in two ways:

- automatically computing a PSF based on known microscopic parameters and a model of the microscope based on electromagnetic diffraction
- or distilling the PSF experimentally from

images of spherical subresolution beads with a spatial frequency content equal or larger than the bandwidth of the microscope

In our experimental set-up the object is embedded in silicon with a refractive index of 3.5 at a wavelength of about 1 micron. As the objective lens is embedded in air this leads to a high refractive index mismatch. Solid immersion lenses (SIL) have been investigated to avoid this mismatch and further improve the numerical aperture and thus the resolution. However it appears very unpractical and expensive as each geometry of a SIL implies a limited focal plane in z , which for an entire z -stack would mean that various SILs would have to be exchanged during the scan. The simulated PSF at different heights in the silicon ($z = 200, 100, 0 \mu\text{m}$) is shown in Figure 5, demonstrating its highly asymmetric nature.

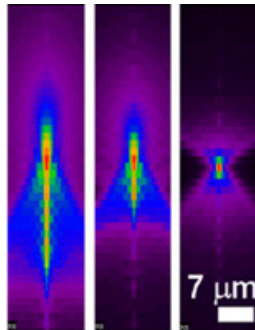


Figure 5: Simulated PSF at different heights inside the silicon substrate, revealing its asymmetric nature. From left to the right: $z = 200, 100$ and $0 \mu\text{m}$.

For obtaining more accurate results Huygens evaluates the appropriate PSF for each layer accounting as well for spherical aberration. In its basic formulation the equation

$$g = h * f + e$$

has to be solved. Where g is the image seen by the CCD camera, e the noise independent from the signal and h the point spread function. f is the original image which has to be restored. Given a model for the PSF f can be estimated. If the difference between the resulting convoluted image and the real image taken has reached the minimum, the estimated f is considered to be the real image, having blurring and noise removed.

The convolution during the estimation process however scales quadratically with the number of volume pixels (voxels), which would lead to long computation times. Therefore the image is transformed to Fourier space and the optical transfer function is evaluated, where the convolution reduces to a multiplication. Fourier transformations are scaling in the order of $N * \log(N)$, where N is the number of voxels.

Once an optical transfer function is provided Huygens can use different mathematical algorithms to effectively solve the convolution equation:

- Classic Maximum Likelihood Estimation
- Quick Maximum Likelihood Estimation
- Iterative Constrained Tikhonov-Miller
- Quick Tikhonov-Miller

which shall not be treated in great detail here.

It shall be mentioned that in the case of wide field microscopy, the optical transfer function has a missing cone of frequencies along the z axis. This makes all the frequencies (both low and high) along this axis to be removed in the convolution imaging process. Frequencies along a line in the Fourier domain represent structures in the perpendicular direction in the spatial domain. The missing cone of frequencies therefore strongly deteriorates the resolution of horizontal structures along the z -axis in the widefield case. These frequencies are in a large part reconstructed by the deconvolution algorithms.

3 THREE DIMENSIONAL REPRESENTATION

During the fusion process in the local contrast based algorithm the respective z -coordinate can be stored. Based on the information of all three coordinates of each pixel, two distinct projections can be calculated with a tilt from the z -axis that can be adjusted to max. 8 degrees. Coding these objects with different colors, red and cyan, and using 3d goggles as known from multimedia, permits a three dimensional impression of the image. In addition an offset, red-cyan-shift, can be adjusted, resulting in an image that appears to come out of the screen or the opposite. An example is given in Figure 6. It shows filaments that are also seen in standard IRM at much lower resolution, and are marked as S2 in Figure 1. The high LIT signal tells that these filaments are heavily shunting.

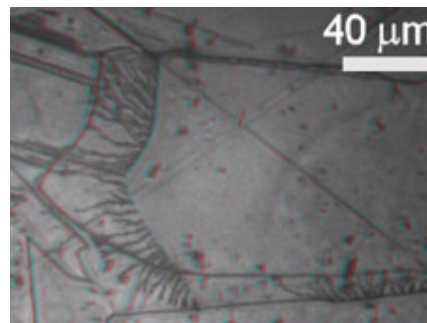


Figure 6: Stereoscopic projection (red-cyan coded) of shunting filaments, marked as S2 in Figure 1. Picolay fusion algorithms was used [8]. (Please use a green-red goggle to see the 3d effect.)

If there are contrast-giving structures in more than one level of the z -stack (as is the case in the solar cells studied here), part of them will remain hidden. Normally, only the pixels giving the highest contrast are displayed. Picolay allows for tilting and even free rotation of the object before the contrast-rich structures are drawn. Hereby masking can be avoided, and all contrast-rich pixels (or, alternatively, those closest to a selected target colour) can be visualised. Again adjustable threshold values are required to avoid that every pixel in all images is displayed and masks underlying layers. For comparison: if one would like to see all occurrences and positions of a certain letter in a book, the paper should be transparent, and one should rotate the book in order to avoid masking. Picolay allows for (animated) rotation of

the projections and recalculates the anaglyphs for each angle.

Figure 7 shows a series of rotations along the x-axis, namely 0, 45, 105 and 135 degrees from the top left to the right bottom. It is the same stack as shown in Figure 2. The images are red-cyan color coded. To support the three dimensional presentation, the height profile is coded from green to yellow. It is clearly shown how the filaments are growing inside grain boundaries. A marker-pen was used to give a better idea on how the surface plane is oriented.

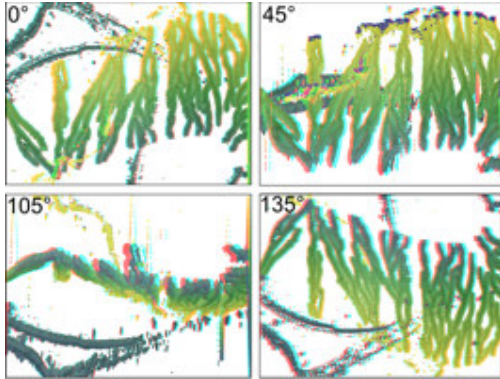


Figure 7: Rotated anaglyphs (red-cyan coded) of SiC filaments from the same stack as shown in Figure 2. Processed with picolay [8].

For 3D volume rendering SVI Huygens offers three different approaches: Maximum Intensity Projections (MIP), Simulated Fluorescence Process (SFP), and iso-data Surface Rendering, based on which also sophisticated animations can be generated. Below we discuss the MIP and SFP methods.

A maximum intensity projection is a volume visualization method for 3d data that projects in the visualization plane the voxels with maximum intensity that fall in the way of rays traced from the viewpoint to the plane of projection. With the viewpoint at infinity, rays become parallel and computation is accelerated. Notice that this implies that two MIP renderings from opposite viewpoints are symmetrical images. This technique is computationally fast but the 2d results do not provide a good sense of depth of the original data. To improve the sense of 3d, animations are usually rendered of several MIP frames in which the viewpoint is slightly changed from one to the other, thus creating the illusion of rotation. This helps the viewer's perception to find the relative 3d positions of the object components. A cropped section from filaments, shown as well in Figure 4, processed by the MIP renderer after deconvolution is shown in Figure 8. The configurable parameters are the rendering size and quality, the appearance of the bounding box, and the mode of the different soft thresholds applied to the image channels.

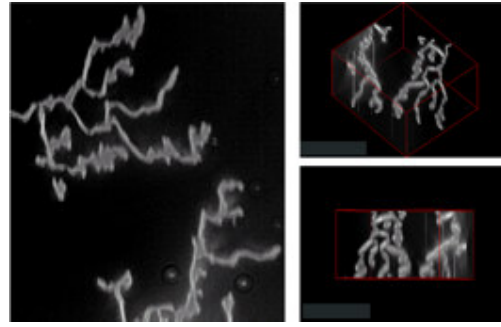


Figure 8: MIP rendered section of filaments as already shown in Figure 4. Huygens deconvolution [9] was applied. On the left a front view as seen from the microscope and on the right various rotations are shown, to demonstrate the tomography-like nature.

In the Simulated Fluorescence Process (SFP) volume rendering algorithm the data is taken as a distribution of fluorescent dyes. By modeling a physical light/matter interaction process an image is computed showing the data as it would have appeared in reality when viewed under these conditions. The algorithm works as follows: In the first stage the fluorescent distribution is illuminated (excited) by a light source at infinity. Because the dye absorbs the excitation light, areas towards the light source will be stronger excited than other areas. Underneath the distribution a flat slab of dye, usually referred to as 'table', is added to visualize cast shadows. In the second stage the light emitted by the distribution and the table propagates towards the viewer. Light which passes through dyes gets absorbed, so areas towards the viewer contribute most to the image. The transparency factors in the excitation and emission phases can be controlled independently.

The unique properties of this algorithm enable it to create depth cue rich images from unprocessed data. Since it does not rely on boundaries or sharp gradients, it is eminently suited to render 3d microscopic data sets. Since the SFP algorithm is based on ray-tracing it does not require a special graphical board as the polygon based techniques do. An example of SFP rendered filaments (the same as in Figure 8) is shown in Figure 9.

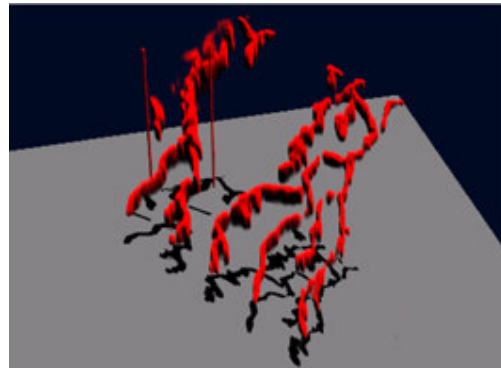


Figure 9: The same section as in Figure 8 is shown, this time SFP rendering [9] is applied, improving the three dimensional impression.

7 SUMMARY

289, 2009.

To improve the resolution of IRM for the imaging of precipitates in mc-Si, objective lenses with high NA have to be used, which decreases drastically the depth of focus. To overcome this problem we presented numeric algorithms to achieve extended depth of focus images at high resolution (below 1 micron). Taking advantage from the additionally gained z-coordinate we present for the very first time tomography-like images and stereoscopic projections of SiC filaments embedded inside the grain boundaries of mc-Si. This method will assist us in the further investigations on the electrical properties and growth mechanisms and SiC filaments and other precipitates, which will become a bigger issue with the introduction of UMG-Si in future.

7 REFERENCES

- [1] O. Breitenstein et al.: Quantitative Evaluation of Shunts in Solar Cells by Lock-in Thermography, *Prog. Photovoltaics: Res. Appl.* 12, 529-538, 2004.
- [2] O. Breitenstein et al.: Shunt types in crystalline silicon solar cells, *Prog. Photovoltaics: Res. Appl.* 12, 529-538, 2004.
- [3] J.P. Rakotoniaina et al., Distribution and Formation of Silicon Carbide and Silicon Nitride Precipitates in Block-Cast Multicrystalline Silicon, *Proceedings 20th European Photovoltaic Solar Energy Conference*, 6-10 June 2005, Barcelona, Spain, 773
- [4] A.K. Søliland et al., SiC and Si₃N₄ inclusions in multicrystalline silicon ingots, *Materials Science in Semiconductor Processing* 7 (2004), 39.
- [5] Hejjo Al Rifai et al., Investigation of material-induced shunts in block-cast multicrystalline silicon solar cells caused by SiC precipitate filaments, *Proceedings 19th European Photovoltaic Solar Energy Conference*, 7-11 June 2004, Paris, France, 632.
- [6] J. Bauer et al., Electronic activity of SiC precipitates in multicrystalline solar silicon, *physica status solidi (a)* 204, No. 7, 2190-2195 (2007), DOI: 10.1002/pssa.200675436.
- [7] A.G. Valdecasas et al., On the extended depth of focus algorithms for bright field microscopy, *Micron* 32, 559-569, 2001.
- [8] www.picolay.de
- [9] www.svi.nl
- [10] R.J. Piper and A. Korpel, Image processing for extended depth of field, *Appl. Opt.* 22, 1449 – 1453, 1983.
- [11] S.A. Sugimoto and Y. Ichioka, Digital composition of images with increased depth of focus considering depth information, *Appl. Opt.* 24, 2076-2080, 1985.
- [12] V. Tympel, A new high level image capture system for conventional light microscopy, *SPIE*, 529-536, 1996.
- [13] N.T. Goldsmith, Deep focus; a digital image processing technique to produce improved focal depth in light microscopy, *Image Anal. Stereol.* 19, 163-167, 2000.
- [14] M. Oberlaender et al., Shack-Hartmann wave front measurements in cortical tissue for deconvolution of large three-dimensional mosaic transmitted light brightfield micrographs, *J. of Microscopy* 233, 275-